

Informative title: Hydraulic redistribution in mangroves: time-lapse electrical resistivity reveals diel patterns of subsurface salt mobilization consistent with exchange of water between trees and sediments

Running title: Time-lapse electrical resistivity reveals diel patterns of salt mobilization

Authors: Christine Downs¹, Ken W. Krauss², Sarah Kruse¹

Affiliations: ¹ University of South Florida, School of Geosciences, 4202 E Fowler Ave, Tampa, FL; ² U.S. Geological Survey, Wetland and Aquatic Research Center, 700 Cajundome Blvd, Lafayette, LA USA

Acknowledgments: Thank you to Rodney Smith, Sajad Jazayeri, Sanaz Esmaeili for assisting with fieldwork; Henok Kiflu and Peter Bumpus for assisting in fieldwork preparation. Thank you to Mark Rains for providing insight about mangrove forest dynamics; and the Smithsonian Marine Station for their generous accommodation and access to the field site. A warm thank you to Marilyn Ball for a careful, expert review of this manuscript. Any use of trade, firm, or product names is for descriptive purposes only and does not imply endorsement by the U.S. government.

Data Availability Statement: The data that support the findings of this study are available from the corresponding author upon reasonable request. If the journal offers a supplemental repository, the author will make the data available.

Abstract

A 24-hour 2D time-lapse electrical resistivity imaging (ERI) survey was conducted in an altered mangrove forest on a barrier island in southeast Florida, USA, to (1) assess the method's utility in hypersaline conditions and (2) understand how trees respond to hypersaline conditions. ERI measurements serve as a proxy for pore water salinity and saturation. Here, resistivity changes suggest a lag between the tidal cycle and changes in ground resistivity. ERI data show that overall changes within 24 hours are very small, but there is more variability in resistivity in the root zone of mangroves than in open salt flat portions along a fixed transect. Two to three hours after sunset, root zone resistivity increased from initial, midday conditions. Overnight, the root zone was less resistive than midday. By sunrise, root zone resistivity was once again higher than initial conditions. Measurements from the salt flat where roots are absent remained generally constant throughout the survey. Thus, changes in resistivity over time are inferred to reflect mangrove tree physiological influences related to diel water use. A mechanistic explanation for the decreased resistivity two hours after sunset from the re-distribution of salts to the soil around the roots is the Cohesion-Tension Theory, which suggests that trees continue water uptake after sunset to balance the pressure after leaf stomates have closed. The corresponding overnight drop in ground resistivity just prior to sunrise may be explained by redistribution of freshwater from the tree to the soil that was delayed until

the early morning hours. The limited period of data acquisition limits definitive data interpretations, but the study illustrates the monitoring potential of ERI in hypersaline environments such as a mangrove forest.

Keywords: 2D, electrical resistivity, groundwater, mangrove, water uptake

Introduction

Mangrove forests are integral components of tropical and subtropical intertidal forest communities and essential to coastal stabilization and ecological processes. Due to their location between land and sea, mangrove forests play a pivotal role in climate change adaptation and mitigation. They show a great deal of ecological stability (Alongi, 2015) through their ability to elevate land surface via sediment accretion and root zone processes, often on pace with sea-level rise (Krauss et al., 2014; McIvor et al., 2013; McKee et al., 2007, 2012). They also have a strong capacity to act as CO₂ sinks (Duarte et al., 2013) while using water conservatively (Lovelock et al., 2006). Their salt tolerance lends mangroves the ability to survive harsh coastal environments (Ball, 1988; Esteban et al., 2013; Parida and Jha, 2010). Some species, like black mangroves (*Avicennia germinans*), rely on foliar salt excretion (Drennan and Pammenter, 1982; Esteban et al., 2013; Parida and Jha, 2010; Scholander et al., 1962) to prevent excess accumulation of salts not excluded when water was absorbed by roots (though black mangrove trees do filter water at the root). Excreted salt on leaves dissolves during cooler, moister periods and returns to the soil during rain events or via excised leaves. Other species, like red (*Rhizophora mangle*) and white (*Laguncularia racemosa*) mangroves, exclude more salt at the roots. During water uptake, water must move down from the soil surface to the roots. By convection, salt also moves down and is then excluded by roots, thus contributing to a local soil salinity maxima directly in the rhizosphere—the region of soil directly influenced by plant root activity (Passioura et al., 1992). While the salt balance in a given tree is presumably maintained, the subsurface can experience gains in salt concentration over time unless upward diffusion of salt balances the downward convection.

Trees may hydrate via foliar absorption of atmospheric water, which can bring more water into the tree than root water uptake alone. This top-down rehydration can ultimately lead to fresh water discharge into the soil. Hao et al. (2009) suggested hydraulic redistribution to explain lower salinities in the root zones of scrub *Rhizophora mangle* that are growing in an area perennially flooded with seawater. Hydraulic redistribution has been demonstrated in many plants of upland ecosystems. Coopman et al. (2021) showed that the capacity of a salt-secreting mangrove (*Avicennia marina*) to access water from an unsaturated atmosphere demonstrates top-down hydration at scales and frequencies of major consequence to tree function under hypersaline conditions. This prompts the questions about the extent and timing of effects of top-down rehydration on soil pore water salinity.

Tidal forcing is typically the dominant mechanism of pore water and salt move-

ment in the saturated and intertidal zones of coastal wetlands and can remove locally excess salt caused by mangrove tree activity (Hughes et al., 1998; Sam and Ridd, 1998; Wolanski et al., 1993). However, the construction of impoundments alters the salinity balance maintained under natural conditions, and, globally, mangroves suffer from tidal restrictions that influence their ecological function and sometimes lead to rapid mortality once multiple stress thresholds are exceeded (Lewis et al., 2016). Impoundments can be earthen dikes that surround sections of forest and hydrologically isolate them from tidal surface water and each other, which can lead to concentrated salinities to levels deleterious even to mangroves. In these cases, evapotranspiration (ET) can become the most influential factor in determining pore water salinities and stand stress, particularly during hot, dry periods (Stringer et al., 2010).

While the concept of root zone salinity concentration with prolonged daily water uptake and ultrafiltration is theoretically tenable, it is important to document how changes in salinity distribution relate to specific tidal and sunrise/sunset cycles in actual mangrove forests. Transpiration significantly decreases at night when photosynthetically active radiation is eliminated, and air temperatures drop. At this time, the water potential in the roots will rise to slow down or cease the intake of soil water. At the start of the day, transpiration resumes, and the root's water potential drops to facilitate root water uptake. Transpiration in mangroves reaches a maximum rate around midday, but maximum cumulative amounts of water transited each day would be realized slightly after sunset as water uptake continues even after stomates (leaf 'pores') are likely closed (Krauss et al., 2007).

This study focuses on an impounded portion of a mangrove forest on a barrier island in east-central Florida, where the forest is isolated from tidal inundation (Figure 1). The impoundment was initially constructed for mosquito abatement. It is comprised of an earthen dike that run along the water's edge and inland to break up the forest into sections. A pump/culvert system is installed within the dike connecting the lagoon to a ditch on the interior side of the dike. In the past, the culvert was a free opening for water to flow through the dike when water levels were high enough. Current water management practices pump brackish water into the impoundment to keep it inundated from April to October to simulate more natural conditions. The impoundment area is then allowed to dry up entirely from November to March.

The trees are predominantly black mangroves and most (90%) porewater salt is excluded during water uptake by the roots. The salt that is transported to the shoot either becomes stored for osmotic adjustment or developing tissues. Excess salt is expelled from the leaves via salt excretion glands (Ball et al., 1988). Impoundment practices can decrease mangrove growth rates and diversity (Berrenstein et al., 2013; Brockmeyer Jr et al., 1996; Crase et al., 2013; Harris et al., 2010; Middleton et al., 2008; Rey et al., 2009, 1990; Rey and Rutledge, 2009), which may imply nutrient limitations, prolonged flooding, and soil hypersalinity within the rhizosphere. In fact, it is typically expected that zones

with the most active roots have the highest salinity concentrations (Passioura et al., 1991) with levels increasing until the rate of convection transport to the roots equal the rate of diffusive transport to the surface sediment. Stringer and others (2010) hypothesized that, in the impoundment of interest, dense, saline pore water in these active zones sinks to create a hypersaline layer 1-4 m below the mangrove and ecophysiological processes within mangrove vegetation such as hydraulic lift (e.g., Dawson, 1993) interact with this layer to alter salinity concentration within the rhizosphere over a daily transpirational cycle. However, in the absence of mangrove activity as ions diffuse along a concentration gradient toward the soil surface such a hypersaline layer would presumably collapse.

We take a geophysical approach to detect spatial and temporal variation in salinity profiles that would reflect diel signatures of water uptake by the trees and hydraulic redistribution of atmospherically-sourced fresh water from the trees into the soil. Time-lapse electrical resistivity imaging (ERI) has proven useful in imaging changes in soil moisture and root uptake (e.g., Beff et al., 2013; Brillante et al., 2016; Consoli et al., 2017; Daily et al., 1992; Garré et al., 2011; Lewis et al., 2016; Mares et al., 2016; Mary et al., 2020; Musgrave and Binley, 2011), the mobility of saline tracers (e.g., Binley et al., 1996; Cassiani et al., 2006; Kemna et al., 2002; Robinson et al., 2020; Singha and Gorelick, 2005; Slater et al., 1997; Slater and Sandberg, 2000) or contaminants (e.g., Hayley et al., 2009; Mansoor and Slater, 2007), and changes in both soil moisture and salinity in saline environments (Attwa et al., 2011; Boaga et al., 2014; Brindt et al., 2019; deFranco et al., 2009; Kiflai et al., 2020; Leroux and Dahlin, 2006; Slater and Sandberg, 2000; Sutter and Ingham, 2016; Urish and Frohlich, 1990; Vacher et al., 2008). This paper reports on the observations made with a time-lapse ERI survey coupled with real-time groundwater data and tidal records. Our objectives were to assess (1) the effectiveness of ERI under hypersaline conditions and (2) the spatiotemporal changes in saline pore water structures as a function of diel and tidal cycles in the absence of surface interaction between the impounded mangrove forest and lagoon. Interpretations were made with consideration given to what is already known about mangrove tree physiological processes in unaltered mangrove forests.

Field Site

Imp-24 is a mosquito-control impoundment on the west side on North Hutchinson Island, Florida, USA (Figure 1 top). North Hutchinson Island is a siliclastic barrier island approximately 35 km long and 0.7 km wide. The Indian River Lagoon, a tidal estuarine system, borders the west shore of the island; the Atlantic Ocean borders the east side. The lagoon connects to the Atlantic Ocean about 9 km south of Imp-24, and a lagged and dampened tidal signature is observed in the ditch between the impoundment and the lagoon compared to the semidiurnal tidal regime observed at the lagoon's opening.

For the Indian River Lagoon, average precipitation rates are 1,180 mm/yr (Sumner and Belaineh, 2005). Open water evaporation rate is 1,502–1,614 mm/yr, with the lowest rate occurring in the winter months (District, 2006; Sumner and

Belaineh, 2005). Vegetated areas experience an estimated 2.6 to 3.5 mm/day (967–1,278 mm/yr) of evapotranspiration based on similar basin mangrove types in the region (Lugo et al., 1975; Twilley and Chen, 1998). Mangrove evapotranspiration (ET) rates strongly influence pore water salinities (Esteban et al., 2013), and changes in water management practices in the mangrove forest have also produced changes in the pore water salinity structure. The vegetation and surface water are separated from the neighboring lagoon by an earthen dike. Maximum water levels are maintained during the summer season (~0.6 m, April–October) and allowed to dry during the winter (November–March) (Connelly and Carlson, 2009; Middleton et al., 2008; Rey and Rutledge, 2009). In the dry season, pore water salinities are more heavily affected by ET rates (Stringer et al., 2010), which lowers the water table and creates a gradient that drives lagoon water to the mangrove via groundwater flow (Figure 1 bottom).

We established a transect through a high-salinity and small-stature mangrove forest. The very shallow subsurface along the resistivity transect can be partitioned into three vegetative zones (Figure 2 top). From the western end to seven meters along the transect, the surface is dominated by dense, height-restricted scrub mangroves. The central portion is a salt flat with standing roots only along the edges. At the center of the salt flat (about 30 m along the transect), there is a small scrub mangrove patch very near the transect. In a sense, much of the salt flat serves as a control area where the influence from root activity is presumably absent. From 40 m along the transect to the eastern end, the vegetation is characterized by sparse, scrub trees. Digging in the vicinity of trees shows the root zones of dense tree groupings extend as far as 1.5 meters in depth. Shallow sediments are fine-grained sand composed of quartz and calcareous grains (Stringer et al., 2010).

Methods

With an AGI Supersting R8 resistivity meter, we performed repeated electrical surveys over 24 hours (March 27–28, 2015) at the end of the "dry" season. Fifty-six electrodes remained stationary throughout the survey. It was important to have high lateral sensitivity in the root zone (0–2 m depth) and moderate vertical sensitivity in the top two meters. Thus, a combined dipole-dipole inverse Schlumberger array configuration with a 1-meter dipole spacing was chosen. Each survey took approximately 45 minutes. To capture both diel and tidal effects on salinity structures in the sub-surface, a 2-D transect array was collected approximately every hour for 24 hours starting at about noon on day 1. Gaps exist in our acquisition schedule due to battery issues. Nevertheless, there is at least one data set representing four diel-tidal combinations—daytime, low tide; daytime, high tide; nighttime, low tide; nighttime, high tide. The first survey acquired 1219 quadripoles; subsequent surveys collected 1045 to 1146 quadripoles for a total of 13,890.

There was standing water at certain times on the western half of the array, so electrodes were cased in PVC pipes pushed approximately 3 cm into the ground to avoid losing current to surface water. Contact resistance tests confirmed

the ground was wet enough to deem watering the electrodes with saltwater unnecessary. Relief along the transect, as observed in a LiDAR-derived digital elevation model, is extremely subtle (0.07 m). For this reason, topography was not included in the inversion.

As in any ER study, it is necessary to assess measurement error before data inversion and interpretation. Following the repeat measurement error assessment of Brindt et al. (2019) and Mares et al. (2016), for example, measurements with an acquisition error above 2% were removed (Figure 2 bottom). Of the 13,890 quadripoles collected, 13,573 were used in the inversion.

The resistivity data were inverted with ResIPy, an open-source geoelectric inversion and modeling software (Blanchy et al., 2020). The models were parameterized on a triangular mesh with the finest node spacing closest to the surface (~0.25 m) and progressively coarser spacing (~1 m) with depth. The first time step was inverted using a uniform reference model of 100 Ωm . Time-lapse inversion is preferred because outliers or noise inherent in each dataset has less influence in the solution versus individual solutions (Binley et al., 1996; Loke, 2014). Time steps were regularized relative to the first dataset to prioritize smoothing changes from one dataset to the next. When the inversion was complete, data points that had a misfit beyond $\pm 3\%$ were filtered out, and the data were inverted again.

Direct groundwater data were also collected using Decagon conductivity, temperature, and water depth sensors (CTD) deployed down PVC wells. The PVC wells, installed four months earlier, were screened at 0.6 m and 1.2 m and resided at the western edge of the transect. Sensors were calibrated at the start of the first day of sampling with room temperature with tap water. The sensors recorded measurements at 15-minute intervals throughout the ERI survey. Due to equipment failure, only water conductivity and one set of temperature readings are presented.

Results and Discussion

The depth of investigation (DOI) was assessed using the method described by Oldenburg and Li (1999), where the first time step is inverted using two different reference resistivities (0.06 and 5.69 Ωm). These reference values were based on the average observed apparent resistivity values. Considering a cautious DOI index cutoff of 0.1, our maximum depth of investigation is about 5 m with the exception of the first 2 m along the array. The true resolution matrix (Figure 3) (Binley and Kemna, 2005, Eq. 5.18) shows inverted resistivity is best resolved in the first 1-2 meters, which is suitable for imaging changes in the root zone of mangrove trees. Accordingly, only the top 2 m of resistivity profiles are presented and discussed.

The inversion results yield zones with near-electrode values that locally alternate between relatively high and low resistivity, particularly at electrodes placed in between tree roots. This is likely due to noisy data as a result of poor contact between electrodes and sediment. Since noise appears to be an issue in vegetated

zones and not the open salt plan, the roots themselves may contribute to poor electrode contact. Small burrowing animals (e.g., fiddler crabs; Ocypodidae) are common in the forest and the distribution of their burrows, which would contribute to poor contact, may be concentrated in the root zone. It is also worth noting that burrowing animal activity also alters local mud chemistry due to enhanced diffusive exchange of dissolved material between the surface and porewater through the sediment surface (Smith et al., 1991).

Since inversion results suffer from near-electrode artifacts, and reciprocal readings were not collected due to time constraints, we present first-order trends and patterns between time-lapse inversion results and environmental changes as measured in ancillary data. Terrain resistivity is controlled by temperature, ground saturation, matrix properties, and groundwater salinity. Results are presented in terms of change from the first time step, thus removing the signature of presumably static matrix properties. The remaining parameters are discussed in turn.

The ground temperature at 0.6 m depth was 22° C at the start of the survey and decreased to 21° C by the end of the survey (Figure 3 bottom). This temperature decrease corresponds to a 2% apparent resistivity increase, which is small but so are resistivity changes between time steps. We use the linear temperature-dependent model from Hayley et al. (2007) and the fractional change coefficient ($m=0.0187$) by Hayashi (2004) to calculate the effect of groundwater temperature at 0.6 m on electrical resistivity measurements. Ground temperature was measured at 15-minute intervals. For a given ERI time step, we averaged ground temperature measurements collected over the duration of a given ERI acquisition time. The temperature-dependent model was applied to each ERI time step using these average values and 22°C as the standard value.

Terrain resistivity is expected to be inversely proportional to the degree of groundwater saturation (e.g., Archie, 1942). There were approximately 4 cm of standing water at the western end of the transect at the start of the study. Surface water levels along this western end gradually dropped until there was no standing water, and did not return through the course of the 24-hour recording period, as would have been expected had the local surface water levels tracked the tidal cycle recorded at the pump station in the trench between the earthen dike and mangrove forest (Locer, 2016) (Figure 4 top). The portion of the forest where the survey took place is thus far enough inland to have not been completely inundated during high tide, and the saturation pattern is not readily correlated with tides. It had rained 18 hours before the study, and standing water levels might also reflect local lateral surface water perching and flow. The ground appeared highly saturated throughout to the end of the study, in the sense that augered holes showed full saturation at depths less than 10 cm.

Pore water resistivity at 0.6 m depth and 1.2 m depth are compared with the mean apparent resistivity from the top 2 meters and easternmost 5 meters along the ERI transect of each time step (Figure 4, middle and bottom, respectively). The ranges of measurement values from 0.6 m and 1.2 m depths are 0.15-0.18 Ω m

and 0.12-0.13 Ωm , respectively. This is a narrower range than that of apparent resistivities (0.01 – 9.23 Ωm) from the west end of the profile. A formation factor is the ratio of the resistivity of water-filled rock or sediment to that of the water and is often used to describe porosity or at least expected porosity for a given geomaterial (Archie, 1942). An average formation factor is estimated here by taking the ratio between water resistivity at 0.6 m depth and the inverted resistivity value for the model cells closest to the location of the 0.6 m well at the east end of the array. Both groundwater conductivity and inverted terrain resistivity were averaged over the diel period, to yield a formation factor of 4.8. This differs from the previous estimate of 3.6 by Stringer et al. (2010), which was based on electromagnetic measurements of terrain conductivity with larger sampling volumes. It has been shown that the formation factor varies spatially and temporally (Singha and Gorelick, 2005), so it is reasonable—and expected—to resolve a range of values at a local scale. The 4.8 value is within the range of published formation factors for sandy soils, such as found at the study site.

Temporal variations in pore water conductivity recorded over the diel period at the wells at 0.6 m and 1.2 m are quite small and not synchronous (Figure 5, middle and bottom). Measurements (converted from conductivity to resistivity for comparative purposes) at 0.6 m correspond to salinities between 38 and 41 psu (Fofonoff and Millard, 1983). Measurements at 1.2 m correspond to above-seawater salinities and are beyond the range of valid values for converting to salinity. The sum of apparent resistivity from each time step is compared to air temperature as well (Figure 5), which helps make inferences about the relationship between ground salinity and saturation and factors that influence ET. Resistivity values for the entire time-lapse survey range from 0.13 to 2600 Ωm . The median resistivity is 2.8 Ωm ; the standard deviation is 1.6 Ωm . Figure 6 shows the change a resistivity between a given time step and the first time step. The values between time steps are quite noisy, as they are relatively small compared to the overall signature. In this study, we focus on first-order trends as they relate to diel and tidal stages within the vegetation zone.

Root zone

Overall, the root zones are more resistive than the neighboring salt flat as expected as roots ameliorate salinity conditions (Figure 6, left column). This applies to the tree groupings on the east and west ends of the resistivity profile and the single shrub in the middle of the profile (Figure 2 top). The patch of standing roots extending out from the western tree grouping away from the forest canopy to about 15 m along the transect is also consistently more resistive than the rest of the salt flat.

We present the difference in inverted resistivity between selected time steps and the initial model at 13:00 during a rising tide (Figure 6, right column). The median difference from the initial model (for all time steps) is 0.22 Ωm , the interquartile range is 0.47 Ωm , and the standard deviation is 1.69 Ωm . Outliers concentrated near selected electrodes are likely due to loss of contact between the electrode and the soil. These values are not shown in Figure 6.

The western tree grouping, including the standing roots extending 15 m into the salt flat, experienced an increase in resistivity (0.5 to 1.3 Ωm increase) from the afternoon until after sunset (22:00) when the tide was falling. This portion of the profile then becomes progressively less resistive until 03:30 (rising tide) when the area is 0.5 to 2 Ωm less resistive than the initial state. From 05:00 to 07:00, conditions are essentially the same as the initial state. After sunrise (08:00 to 11:00), the western tree grouping and standing roots are once again more resistive than the initial conditions though not to the same extent as the previous afternoon and evening.

The single shrub in the middle of the salt flat presents a similar trend. Conditions are more resistive than the initial state through the afternoon and early evening. Resistivity decreases until the early morning hours when conditions are similar to or less resistive than the initial state. The area is once again more resistive after sunrise. The eastern tree grouping consistently yields very large changes from the initial model. Although outliers are present, the overall trend suggests the area is more resistive than initial conditions during the day and less resistive overnight.

Interpretations

The temporal changes in the resistivity profiles are on the same scale as those in the measured groundwater conductivities over the diel period (Figure 4); however, they do not necessarily follow the same trend. Such small changes in ground conductivities, as measured in the ER data, fall in the envelope of instrument error (± 0.01 mS/cm or $\pm 1e3$ Ωm .) The overall values do yield a plausible formation factor, and the higher pore water resistivities recorded at 0.6-meter depth over those at 1.2-meters depth agree with the distribution recorded in the resistivity surveys. The terrain resistivity data are robust in that they agree with the observed geological structure and show general trends that can be interpreted.

In a coastal environment, one can expect shallow terrain resistivities to be their lowest at high tide when tidal forcing increases the extent of brackish water ingress. Although the impoundment does not experience tidal inundation, we considered any signature of tidal forcing. In this study, the lowest resistivities are observed overnight after high tide as the tide is falling (Figure 4; Figure 6, right column). This would indicate that the tidal cycle does influence ground resistivity and that there is a time lag between high tide and minimum ground resistivity. On the other hand, the same pattern is not observed before sunset when the tide is also falling. Furthermore, this pattern is not captured by direct groundwater measurements. Thus, our observations do not appear to support tidal cycles as the sole controller of the observed resistivity cycle. We consider instead that our ER data are, at least partially, controlled by pore water conductivity and saturation changes, which are, to some extent, controlled by tree activity and varies with the time of day.

Low water pressure potential in roots creates an upward hydraulic gradient

during daylight hours. Black mangrove trees partially filter salts at the root during water uptake and excrete excess salt from the leaves during transpiration. Transpiration rates of south Florida mangrove trees slow down with stomatal closure at sundown, but upward stem water movement (sap flow) continues one to two hours in many tree species after sunset as continued water absorption is required for rehydration of tissues in an effort to balance the pressure well after stomates are closed (Meinzer et al., 2004). Black mangroves growing in scrub environments of Louisiana, USA continue to take water up for at least an hour or more after sunset (Krauss et al., 2014). The water pressure gradient in a tree is inversely proportional to its water content. Accordingly, the sustained upward sap flow can continue until the pressure gradient between soil pore water and the tree collapses. Recharge of the soil possible if the tree achieves a higher water potential than that of pore water around the roots. A possible scenario for this could be the uptake of water from roots at shallow soil depths where pore water salinity is lower than that of soil pore water surrounding roots at greater soil depths. This may lead to a downward transfer, via reverse sap flow, of low salinity water extracted from shallow soil depths and transported through the tree into greater soil depths. Whether reverse sap flow occurs or not, transpiration resumes at sunrise prompting the upward hydraulic gradient once again.

If we consider this cycle in terms of the resistivity results, some patterns emerge. Relative to the first time step at 15:00, the root zone became more resistive in the late afternoon before sunset (Figure 6, right column). These conditions continued— though a slight decrease in resistivity is present after sunset (19:30)— until approximately midnight. Recall that black mangrove trees exclude 90% of pore water salts during water uptake. We attribute the increased resistivity to continual water uptake of filtered water stranding salts in the rhizosphere, suggesting the ER response is from a combination of declining water content and increased soil salinity. The trend continues throughout the first half of the night as sap flow is known to also continue. Boaga et al. (2014), for example, also show that water uptake in the root zone can produce pockets of more resistive ground even when the surface is flooded.

From about midnight to sunrise, the ground is overall less resistive than initial conditions. The largest decreases occurring in vegetated areas. The salt flat is only slightly less resistive than initial conditions (about $-0.25 \Omega\text{m}$) and the change is very uniform. In a sense, the salt flat where roots are completely absent serve as a control area. We attribute the larger decrease in resistivity to water uptake ceasing and even freshwater recharge to the area around trees via reverse sap flow (e.g. Coopman et al., 2021). Again, this suggests that varying water content is driving the ER signal.

Ground conditions are once again more resistive than initial conditions by sunrise (07:30). The pattern in increased resistivity is similar to that pre-sunset with the most significant changes occurring in vegetated and standing root areas. These conditions continue through to the end of the survey (11:00). We

attribute this to transpiration resuming, prompting an upward hydraulic gradient and water uptake.

The suggestion of water returning to the soil via tree roots is the process known as hydraulic redistribution that has been observed in dry environments (Caldwell et al., 1998; Caldwell and Richards, 1989; Ludwig et al., 2003; Richards and Caldwell, 1987), temperate forests (Meinzer et al., 2004), savannas (Meinzer et al., 2004; Scholz et al., 2002) and mangrove forests (Hao et al., 2009). Hao and others (2009) found that reverse flow in dwarf red mangroves in south Florida may help to relieve the adverse effects of hypersaline conditions in a given tree. Our results support this process. While the hypersaline conditions in the impounded mangrove forest discuss here are detrimental to mangrove tree growth, hydraulic redistribution may be an important factor in addition to salt exclusion and salt excretion for its survival (Figure 7).

The mangrove trees may then reverse their pressure gradient overnight rather than simply reduce water uptake completely and redistribute freshwater to the root zone slowly thereafter, perhaps in combination with high tide. Such a phenomenon would indicate mangrove trees benefit from hydraulic redistribution overnight to offset maximum transpiration-imposed root zone salinity increases by the end of the day and into the early part of the evening. This would require an alternative source of water, specifically uptake of atmospheric water.

Our study tests the ability of electrical resistivity to detect small changes in ground resistivity in a hypersaline environment. The observations presented here are temporally finite. It is not possible to make inferences about seasonal or annual patterns or even average daily processes. Nevertheless, the data indicate a tidal influence compounded with mangrove tree physiological processes, understanding of which ultimately assists in assessing the long-term effects of diking on mangrove forests.

Conclusions

We evaluate the use of repeat electrical resistivity surveys to image changing ground conditions in a hypersaline mangrove environment. Time-lapse electrical resistivity surveys capture dynamic processes within the root zone of a mangrove forest over a diel cycle and appear to reflect tree physiological processes and tidal forcing. We infer that the mangrove trees in an impounded forest on a barrier island may pull saline water up from the root zone during the day and for a time after sunset. The data suggest that this process reverses overnight when fresher water is returned to the soil via hydraulic redistribution. The period over which data acquisition took place limits data interpretations and the data appears to suffer from noise due to questionable contact between electrodes and sediment. Nevertheless, this study presents the utility of ER in monitoring plant-soil interactions in hypersaline environments, such as a mangrove forest.

References

Alongi, D.M., 2015. The impact of climate change on mangrove forests. *Curr. Clim. Chang. Reports* 1, 30–39.

Archie, G.E., 1942. The electrical resistivity log as an aid in determining some reservoir characteristics. *Trans. AIME* 146, 54–62.

Attwa, M., Günther, T., Grinat, M., Binot, F., 2011. Evaluation of DC, FDEM and IP resistivity methods for imaging perched saltwater and a shallow channel within coastal tidal flat sediments. *J. Appl. Geophys.* 75, 656–670. <https://doi.org/10.1016/j.jappgeo.2011.09.002>

Ball, M.C., 1988. Ecophysiology of mangroves. *Trees* 2, 129–142.

Beff, L., Günther, T., Vandoorne, B., Couvreur, V., Javaux, M., 2013. Three-dimensional monitoring of soil water content in a maize field using electrical resistivity tomography. *Hydrol. Earth Syst. Sci.* 17. <https://doi.org/10.5194/hess-17-595-2013>

Berrenstein, H.J., Mans, D.R.A., Bhansing, M., Wakiran, W.S., Atmopawiro, S.L., Chotkan, N.R., Karsoredjo, R.S., Sabiran, S.A., 2013. Effects of diking on the biological performance of the black mangrove (*Avicennia germinans* L.) in an Atlantic mangrove forest. *Wetl. Ecol. Manag.* 21, 165–172.

Binley, A., Henry-Poulter, S., Shaw, B., 1996. Examination of solute transport in an undisturbed soil column using electrical resistance tomography. *Water Resour. Res.* 32, 763–769.

Binley, A., Kemna, A., 2005. DC Resistivity and Induced Polarization Methods, in: *Hydrogeophysics*. https://doi.org/10.1007/1-4020-3102-5_5

Blanchy, G., Saneiyani, S., Boyd, J., McLachlan, P., Binley, A., 2020. ResIPy, an intuitive open source software for complex geoelectrical inversion/modeling. *Comput. Geosci.* <https://doi.org/10.1016/j.cageo.2020.104423>

Boaga, J., D’Alpaos, A., Cassiani, G., Marani, M., Putti, M., 2014. Plant-soil interactions in salt marsh environments: Experimental evidence from electrical resistivity tomography in the Venice Lagoon. *Geophys. Res. Lett.* 41. <https://doi.org/10.1002/2014GL060983>

Brillante, L., Bois, B., Mathieu, O., Lévêque, J., 2016. Electrical imaging of soil water availability to grapevine: a benchmark experiment of several machine-learning techniques. *Precis. Agric.* 17. <https://doi.org/10.1007/s11119-016-9441-1>

Brindt, N., Rahav, M., Wallach, R., 2019. ERT and salinity – A method to determine whether ERT-detected preferential pathways in brackish water-irrigated soils are water-induced or an artifact of salinity. *J. Hydrol.* 574. <https://doi.org/10.1016/j.jhydrol.2019.04.029>

Brockmeyer Jr, R.E., Rey, J.R., Virnstein, R.W., Gilmore, R.G., Earnest, L., 1996. Rehabilitation of impounded estuarine wetlands by hydrologic reconnection to the Indian River Lagoon, Florida (USA). *Wetl. Ecol. Manag.* 4, 93–109.

Caldwell, M.M., Dawson, T.E., Richards, J.H., 1998. Hydraulic lift: consequences of water efflux from the roots of plants. *Oecologia* 113, 151–161.

Caldwell, M.M., Richards, J.H., 1989. Hydraulic lift: water efflux from upper roots improves effectiveness of water uptake by deep roots. *Oecologia* 79, 1–5.

Cassiani, G., Bruno, V., Villa, A., Fusi, N., Binley, A., 2006. A saline trace test monitored via time-lapse surface electrical resistivity tomography. *J. Appl. Geophys.* 59, 244–259.

Connelly, C.R., Carlson, D.B. (Eds.), 2009. *Florida Mosquito Control: The state of the mission as defined by mosquito controllers, regu-*

lators, and environmental managers., Florida Co. ed. University of Florida, Institute of Food and Agriculture Sciences, Florida Medical Entomology Laboratory, Vero Beach, FL.Consoli, S., Stagno, F., Vanella, D., Boaga, J., Cassiani, G., Rocuzzo, G., 2017. Partial root-zone drying irrigation in orange orchards: Effects on water use and crop production characteristics. *Eur. J. Agron.* <https://doi.org/10.1016/j.eja.2016.11.001>Coopman, R.E., Nguyen, H.T., Mencuccini, M., Oliveira, R.S., Sack, L., Lovelock, C.E. and Ball, M.C., 2021. Harvesting water from unsaturated atmospheres: deliquescence of salt secreted onto leaf surfaces drives reverse sap flow in a dominant arid climate mangrove, *Avicennia marina*. *New Phytologist*, *231*(4), pp.1401-1414.Crase, B., Liedloff, A., Vesk, P.A., Burgman, M.A., Wintle, B.A., 2013. Hydroperiod is the main driver of the spatial pattern of dominance in mangrove communities. *Glob. Ecol. Biogeogr.* *22*, 806–817.Daily, W., Ramirez, A., LaBrecque, D., Nitao, J., 1992. Electrical resistivity tomography of vadose water movement. *Water Resour. Res.* *28*, 1429–1442. <https://doi.org/10.1029/91WR03087>Dawson, T.E., 1993. Hydraulic lift and water use by plants: implications for water balance, performance and plant-plant interactions. *Oecologia* *95*. <https://doi.org/10.1007/BF00317442>deFranco, R., Biella, G., Tosi, L., Teatini, P., Lozej, A., Chiozzotto, B., Giada, M., Rizzetto, F., Claude, C., A., M., and Bassan, V., Gasparetto-Stori, G., 2009. Monitoring the saltwater intrusion by time lapse electrical resistivity tomography: The Chioggia test site (Venice Lagoon, Italy). *J. Appl. Geophys.* *69*, 117–130. <https://doi.org/10.1016/j.jappgeo.2011.08.004>District, S.J.R.W.M., 2006. Evaluation of potential impact of demineralization concentration discharge to the Indian River Lagoon (study).Drennan, P., Pammenter, N.W., 1982. Physiology of salt excretion in the mangrove *Avicennia marina* (Forsk.) Vierh. *New Phytol.* *91*, 597–606.Duarte, C.M., Losada, I.J., Hendriks, I.E., Mazarrasa, I., Marbà, N., 2013. The role of coastal plant communities for climate change mitigation and adaptation. *Nat. Clim. Chang.* *3*. <https://doi.org/10.1038/NCLIMATE1970>Esteban, R., Fernández-Marin, B., Hernandez, A., Jiménez, E.T., León, A., García-Mauriño, S., Silva, C.D., Dolmus, J.R., Dolmus, C.M., Molina, M.J., Others, 2013. Salt crystal deposition as a reversible mechanism to enhance photoprotection in black mangrove. *Trees* *27*, 229–237.Fofonoff, N.P., Millard, R.C., 1983. Algorithms for computation of fundamental properties of seawater. *UNESCO Tech. Pap. Mar. Sci.* *44*. <https://doi.org/10.1111/j.1365-2486.2005.001000.x>Garré, S., Javaux, M., Vanderborght, J., Pagès, L., Vereecken, H., 2011. Three-dimensional electrical resistivity tomography to monitor root zone water dynamics. *Vadose Zo. J.* <https://doi.org/10.2136/vzj2010.0079>Hao, G.-Y., Jones, T.J., Luton, C., Zhang, Y.-J., Manzane, E., Scholz, F.G., Bucci, S.J., Cao, K.-F., Goldstein, G., 2009. Hydraulic redistribution in dwarf *Rhizophora* mangrove trees driven by interstitial soil water salinity gradients: impacts on hydraulic architecture and gas exchange. *Tree Physiol.* *29*, 697–705.Harris, R.J., Milbrandt, E.C., Everham III, E.M., Bovard, B.D., 2010. The effects of reduced tidal flushing on mangrove structure and function across a disturbance gradient. *Estuaries and coasts* *33*, 1176–1185.Hayashi,

M., 2004. Temperature-electrical conductivity relation of water for environmental monitoring and geophysical data inversion. *Environ. Monit. Assess.* 96, 119–128. <https://doi.org/10.1023/B:EMAS.0000031719.83065.68>

Hayley, K., Bentley, L.R., Gharibi, M., 2009. Time-lapse electrical resistivity monitoring of salt-affected soil and groundwater. *Water Resour. Res.* 45. <https://doi.org/10.1029/2008WR007616>

Hayley, K., Bentley, L.R., Gharibi, M., Nightingale, M., 2007. Low temperature dependence of electrical resistivity: Implications for near surface geophysical monitoring. *Geophys. Res. Lett.* 34.

Hughes, C.E., Binning, P., Willgoose, G.R., 1998. Characterisation of the hydrology of an estuarine wetland. *J. Hydrol.* 211, 34–49.

Kemna, A., Vanderborght, J., Kulesa, B., Vereecken, H., 2002. Imaging and characterisation of subsurface solute transport using electrical resistivity tomography ERT and equivalent transport models. *J. Hydrol.* 267, 125–146.

Kiflai, M.E., Whitman, D., Ogurcak, D.E., Ross, M., 2020. The Effect of Hurricane Irma Storm Surge on the Freshwater Lens in Big Pine Key, Florida using Electrical Resistivity Tomography. *Estuaries and Coasts* 43. <https://doi.org/10.1007/s12237-019-00666-3>

Krauss, K.W., McKee, K.L., Lovelock, C.E., Cahoon, D.R., Saintilan, N., Reef, R., Chen, L., 2014. How mangrove forests adjust to rising sea level. *New Phytol.* 202, 19–34.

Krauss, K.W., Young, P.J., Chambers, J.L., Doyle, T.W., Twilley, R.R., 2007. Sap flow characteristics of neotropical mangroves in flooded and drained soils. *Tree Physiol.* 27, 775–783.

Leroux, V., Dahlin, T., 2006. Time-lapse resistivity investigations for imaging saltwater transport in glaciofluvial deposits. *Environ. Geol.* 49, 347–358. <https://doi.org/10.1007/s00254-005-0070-7>

Lewis, R.R., Milbrandt, E.C., Brown, B., Krauss, K.W., Rovai, A.S., Beever, J.W., Flynn, L.L., 2016. Stress in mangrove forests: Early detection and preemptive rehabilitation are essential for future successful worldwide mangrove forest management. *Mar. Pollut. Bull.* 109. <https://doi.org/10.1016/j.marpolbul.2016.03.006>

Locer, E., 2016. Locer Environmental [WWW Document]. URL <http://data.locherenv.com/vdv/index.php>

Loke, M.H., 2014. Time-lapse resistivity imaging inversion, in: 5th EEGS-ES Meeting. <https://doi.org/10.3997/2214-4609.201406397>

Lovelock, C.E., Ball, M.C., Feller, I.C., Engelbrecht, B.M.J., Ewe, M.L., Ling Ewe, M., 2006. Variation in hydraulic conductivity of mangroves: influence of species, salinity, and nitrogen and phosphorus availability. *Physiol. Plant.* 127, 457–464.

Ludwig, F., Dawson, T.E., de Kroon, H., Berendse, F., Prins, H.H.T., 2003. Hydraulic lift in *Acacia tortilis* trees on an East African savanna. *Oecologia* 134, 293–300.

Lugo, A.E., Evink, G., Brinson, M.M., Broce, A., Snedaker, S.C., 1975. Diurnal rates of photosynthesis, respiration, and transpiration in mangrove forests of south Florida, in: Golley, F.B., Medina, E. (Eds.), *Tropical Ecological Systems*, Vol. 11. Springer, pp. 335–350. https://doi.org/https://doi.org/10.1007/978-3-642-88533-4_22

Mansoor, N., Slater, L., 2007. Aquatic electrical resistivity imaging of shallow-water wetlands. *Geophysics* 72, F211–F221.

Mares, R., Barnard, H.R., Mao, D., Revil, A., Singha, K., 2016. Examining diel patterns of soil and xylem moisture using electrical resistivity imaging. *J. Hydrol.* 536. <https://doi.org/10.1016/j.jhydrol.2016.03.003>

Mary, B., Peruzzo, L.,

Boaga, J., Cenni, N., Schmutz, M., Wu, Y., Hubbard, S.S., Cassiani, G., 2020. Time-lapse monitoring of root water uptake using electrical resistivity tomography and mise-à-la-masse: a vineyard infiltration experiment. *SOIL* 6, 95–114. <https://doi.org/10.5194/soil-6-95-2020>

McIvor, A.L., Spencer, T., Möller, I., Spalding, M., 2013. The response of mangrove soil surface elevation to sea level rise. *Nat. Coast. Prot. Ser. Rep. 3*. Cambridge Coastal Res. Unit Work. Pap. 42. ISSN 2050-7941.

McKee, K., Rogers, K., Saintilan, N., 2012. Response of salt marsh and mangrove wetlands to changes in atmospheric CO₂, climate, and sea level, in: *Global Change and the Function and Distribution of Wetlands*. https://doi.org/10.1007/978-94-007-4494-3_2

McKee, K.L., Cahoon, D.R., Feller, I.C., 2007. Caribbean mangroves adjust to rising sea level through biotic controls on change in soil elevation. *Glob. Ecol. Biogeogr.* 16. <https://doi.org/10.1111/j.1466-8238.2007.00317.x>

Meinzer, F.C., Brooks, J.R., Bucci, S., Goldstein, G., Scholz, F.G., Warren, J.M., 2004. Converging patterns of uptake and hydraulic redistribution of soil water in contrasting woody vegetation types. *Tree Physiol.* 24, 919–928.

Middleton, B., Devlin, D., Proffitt, E., McKee, K., Cretini, E.F., 2008. Characteristics of mangrove swamps managed for mosquito control in eastern Florida, USA. *Mar. Ecol. Prog. Ser.* 371, 117–129.

Musgrave, H., Binley, A., 2011. Revealing the temporal dynamics of subsurface temperature in a wetland using time-lapse geophysics. *J. Hydrol.* 396. <https://doi.org/10.1016/j.jhydrol.2010.11.008>

Oldenburg, D.W., Li, Y., 1999. Estimating depth of investigation in DC resistivity and IP surveys. *Geophysics* 64, 403–416. <https://doi.org/10.1190/1.1444545>

Parida, A.K., Jha, B., 2010. Salt tolerance mechanisms in mangroves: A review. *Trees* 24, 199–217.

Passioura, J. B., M. C. Ball, and J. H. Knight. 1992. Mangroves may salinize the soil and in so doing limit their transpiration rate. *Functional Ecology.* 6, 4, 476-481. <https://doi.org/10.2307/2389286>

Rada, F., Goldstein, G., Orozco, A., Montilla, M., Zabala, O., Azocar, A., 1989. Osmotic and turgor relations of three mangrove ecosystem species. *Funct. Plant Biol.* 16, 477–486.

Rey, J.R., O’Connell, S.M., Carlson, D.B., Brockmeyer Jr, R.E., 2009. Characteristics of mangrove swamps managed for mosquito control in eastern Florida, USA: a re-examination. *Mar. Ecol. Prog. Ser.* 389, 295–300.

Rey, J.R., Rutledge, C.R., 2009. Mosquito Control Impoundments. *Entomol. Nematol.*

Rey, J.R., Shaffer, J., Crossman, R., Tremain, D., 1990. Above-ground primary production in impounded, ditched, and natural *Batis-salicornia* marshes along the Indian River Lagoon, Florida, USA. *Wetlands* 10, 151–171.

Richards, J.H., Caldwell, M.M., 1987. Hydraulic lift: substantial nocturnal water transport between soil layers by *Artemisia tridentata* roots. *Oecologia* 73, 486–489.

Robinson, J., Buda, A., Collick, A., Shoher, A., Ntarlagiannis, D., Bryant, R., Folmar, G., Andres, S., Slater, L., 2020. Electrical monitoring of saline tracers to reveal subsurface flow pathways in a flat ditch-drained field. *J. Hydrol.* <https://doi.org/10.1016/j.jhydrol.2020.124862>

Sam, R., Ridd, P., 1998. Spatial variations of groundwater salinity in a mangrove-salt flat system, Cocoa Creek, Australia. *Mangroves Salt Marshes* 2, 121–132.

Scholander, P.F., Hammel, H.T., Hemmingsen, E., Garey, W., 1962. Salt balance in mangroves. *Plant Physiol.* 37, 722.

Scholz, F.G., Bucci, S.J., Guillermo, G.,

and Meinzer, F.C., Franco, A.C., 2002. Hydraulic redistribution of soil water by neotropical savanna trees. *Tree Physiol.* 22, 603–612.

Singha, K., Gorelick, S.M., 2005. Saline tracer visualized with three-dimensional electrical resistivity tomography: Field-scale spatial moment analysis. *Water Resour. Res.* <https://doi.org/10.1029/2004WR003460>

Slater, L., Binley, A.M., Daily, W., Johnson, R., 2000. Cross-hole electrical imaging of a controlled saline tracer injection. *J. Appl. Geophys.* [https://doi.org/10.1016/S0926-9851\(00\)00002-1](https://doi.org/10.1016/S0926-9851(00)00002-1)

Slater, L., Zaidman, M.D., Binley, A.M., West, L.J., 1997. Electrical Imaging of Saline Tracer Migration for the Investigation of Unsaturated Zone Transport Mechanisms. *Hydrol. Earth Syst. Sci.* <https://doi.org/10.5194/hess-1-291-1997>

Slater, L.D., Sandberg, S.K., 2000. Resistivity and induced polarization monitoring of salt transport under natural hydraulic gradients. *GEOPHYSICS.* <https://doi.org/10.1190/1.1444735>

Smith III, T.J., Boto, K.G., Frusher, S.D. and Giddins, R.L., 1991. Keystone species and mangrove forest dynamics: the influence of burrowing by crabs on soil nutrient status and forest productivity. *Estuarine, coastal and shelf science*, 33(5), pp.419-432.

Stringer, C.E., Rains, M.C., Kruse, S., Whigham, D., 2010. Controls on water levels and salinity in a barrier island mangrove, Indian River Lagoon, Florida. *Wetlands* 30, 725–734.

Sumner, D.M., Belaine, G., 2005. Evaporation, precipitation, and associated salinity changes at a humid, subtropical estuary. *Estuaries* 28, 844–855.

Sutter, E., Ingham, M., 2016. Seasonal saline intrusion monitoring of a shallow coastal aquifer using time-lapse DC resistivity traversing. *Near Surf. Geophys.* 14, 1–15. <https://doi.org/10.3997/1873-0604.2016039>

Twilley, R.R., Chen, R., 1998. A water budget and hydrology model of a basin mangrove forest in Rookery Bay, Florida. *Mar. Freshw. Res.* 49, 309–323.

Urish, D.W., Frohlich, R.K., 1990. Surface electrical resistivity in coastal groundwater exploration. *Geoexploration* 26, 267–289.

Vacher, H.L., Seale, L.D., Florea, L.J., Brinkmann, R., 2008. Using ALSM to map sinkholes in the urbanized covered karst of Pinellas County, Florida—2. Accuracy statistics. *Environ. Geol.* 54, 1007–1015.

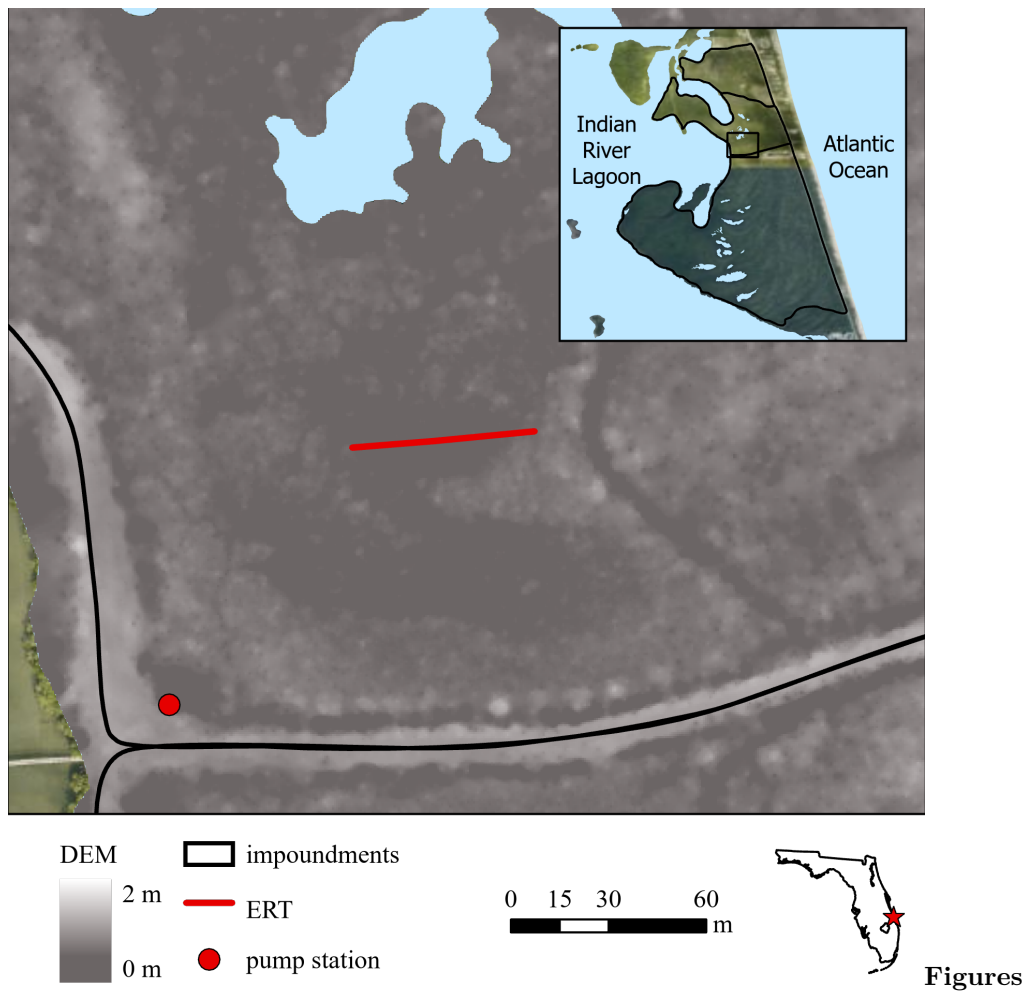
Wolanski, E., Mazda, Y., Ridd, P., 1993. Mangrove hydrodynamics. *Trop. mangrove Ecosyst.* 43–62.

Tables

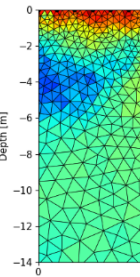
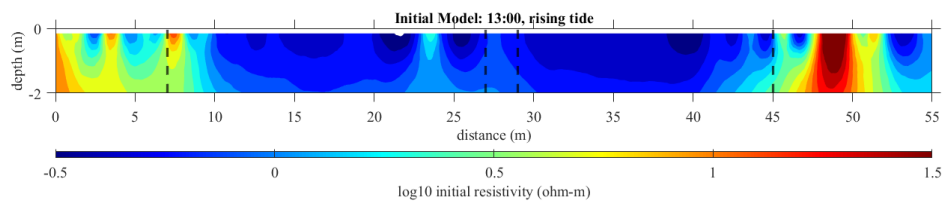
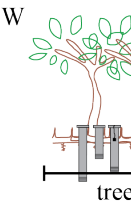
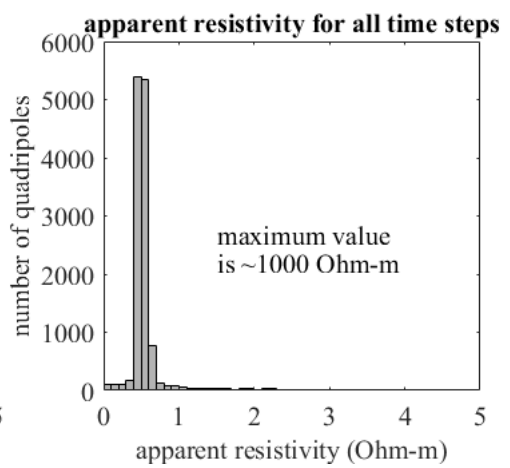
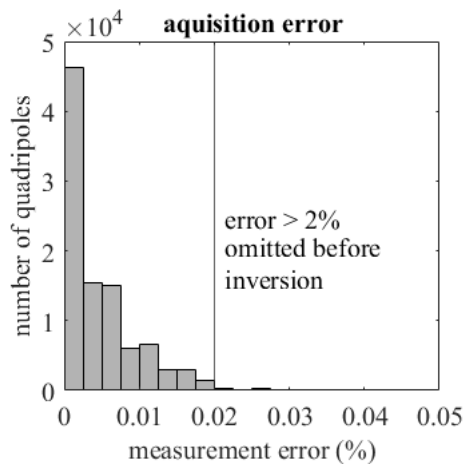
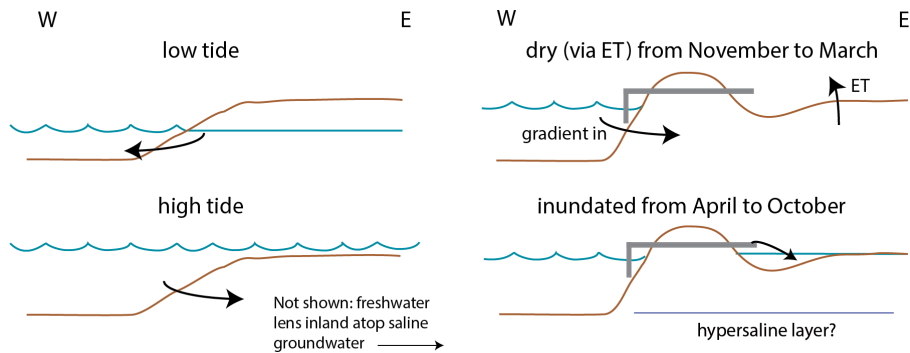
Time Step	Start	End	Duration	Quadripoles		
1	12:18:39	13:05:49	0:47:10	1219	day 1	rising tide
2	13:46:05	14:32:37	0:46:32	1146		
3	18:45:29	19:31:38	0:46:09	1049		falling tide
4	19:32:57	20:19:34	0:46:37	1047	night	
5	20:29:51	21:16:41	0:46:50	1048		
6	21:20:37	22:08:00	0:47:23	1048		
7	0:01:16	0:47:28	0:46:12	1048		rising tide
8	3:09:18	3:57:04	0:47:46	1049		
9	4:40:01	5:26:26	0:46:25	1048		
10	6:38:22	7:26:26	0:48:04	1049		falling tide
11	7:44:00	8:30:43	0:46:43	1045	day 2	

Time Step	Start	End	Duration	Quadripoles
12	8:34:44	9:22:03	0:47:19	1049
13	10:45:12	11:34:33	0:49:21	1045

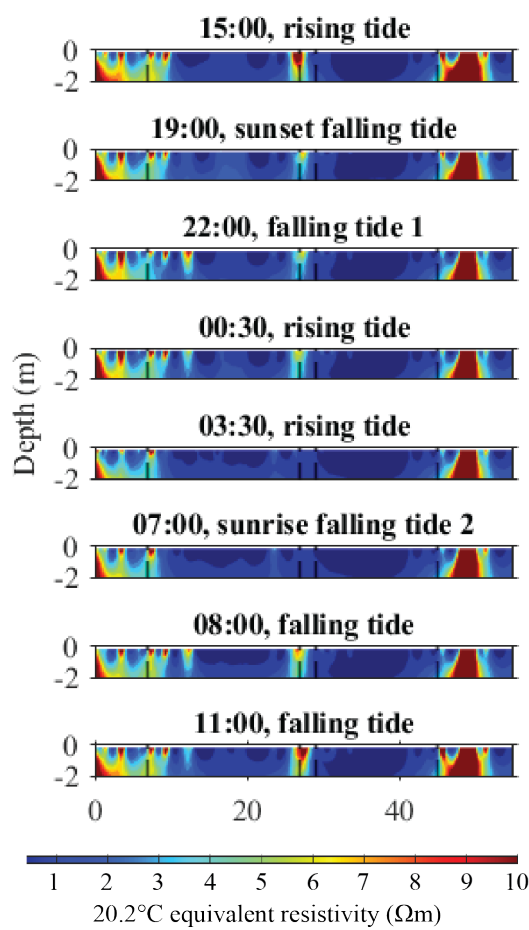
Table 1 Data acquisition schedule. Only time steps that shown significant change (**bold**) from the initial time step (*italics*) are presented in this paper.



Figures



[CHART][CHART][CHART]



[CHART]

